Boris Delipetar ✉
Ivana Weber
Damir Kovačić

https://doi.org/10.21278/TOF.502086326
ISSN 1333-1124
eISSN 1849-1391

SEM/EDS CHARACTERISATION OF MEA SUBSTRATES WITH 3D MICROTOPOGRAPHY: COMPOSITION UNIFORMITY METRICS AND SALT-RESIDUE COVERAGE

Summary

This study presents the characterisation of microelectrode array (MEA) chips with 3D microtopography using scanning electron microscopy (SEM) and energy-dispersive X-ray spectroscopy (EDS). The aim was to evaluate the uniformity of the composition across four microtopographic zones and between individual chips, as well as to assess surface coverage following the drying of Neurobasal-A (NB-A) culture medium. The atomic fractions of the chip elements were expressed by the titanium ratio (Ti_index) on three chips. The residue coverage of the chip surface with dried NB-A droplets on a four-chip sample (3 or 30 µL; two chips per volume) was expressed by NaCl_index (Na and Cl relative to chip-related elements). A two-factor ANOVA test showed a tendency for the Ti_index to vary across zones rather than between chips, implying a high-quality manufacturing process. The NaCl_index increased with the volume of the culture medium without a noticeable effect across zones, indicating that the dried medium may mask the microstructures of the chip surface.

Key words: *microelectrode array (MEA); microstructured topography; energy-dispersive X-ray spectroscopy (EDS); surface characterisation*

1. Introduction

Microelectrode array (MEA) platforms are a proven and widespread technology in extracellular electrophysiology of neuronal cultures. However, the reliability of recording and stimulation depends on cell-electrode coupling, which is affected by the electrode material, surface cleanliness and quality, and geometry uniformity. Modern MEA systems feature a high density of electrodes and high complexity of the interface [1-5], which requires precise characterisation of the substrate surfaces from the aspect of the quality of the production process.

The introduction of three-dimensional topography of the surface of the electrodes and the substrate surrounding them has proven to be one of the successful approaches to improving the coupling. In an extensive doctoral thesis, Huys designed and implemented a process for the fabrication and integration of high-density MEA substrates using surface micropillars on the surface of the chip as a substrate [6]. Following on from the initial research, 16k Complementary Metal-Oxide-Semiconductor (CMOS) MEAs were presented for single-cell electrophysiological tests at the extracellular level [7]. The same research group demonstrated

localised stimulation on active MEAs, showing how 3D microelectrodes can influence the extracellular readout toward intracellular-like signal shapes, highlighting the importance of interface reproducibility with microscale electrodes [8, 9].

Microtopographic substrates have been widely investigated from the aspect of their influence on cell growth and on the development and improvement of cell-substrate interaction through the mediation of mechanotaxis, i.e., the mechanism of cell guidance via mechanical cues [10-13]. Substrates with micropillars in auditory neuroelectronics have shown the ability to influence the morphology of spiral ganglion neurons (SGNs) and induce the geometry-dependent growth and orientation of neurites, supporting the premise that microtopography can directly improve cell-substrate interactions [14-16]. In the continuation of the research, a proof-of-concept neuroelectronic interface (NEI) was demonstrated with the integrated microtopography of the MEA substrate and enabling extracellular recording and stimulation of neurons [17], which requires careful control of the quality of the substrate.

Scanning electron microscopy (SEM) coupled with energy-dispersive X-ray spectroscopy (EDS) represents the standard method for the characterisation and verification of microfabricated surface topography, as well as for the detection of substrate contamination and elemental composition analysis. Recent advances in methodology have improved EDS quantification and mapping protocols, with emphasis given to the role of absorption and geometry effects on acquisition precision [18]. However, SEM and EDS techniques on 3D surfaces at the micro and nanoscale are sensitive to the geometry of the surface (take-off angle, shadowing), which can negatively affect the reliability of the reading of atomic fractions when the field of view (FOV) includes different materials and variations in heights [19-23]. These limitations are particularly evident in the microtopography of MEA substrates, where densely spaced micropillars and electrodes create surface relief that can impair effective X-ray visibility. Therefore, the use of robust descriptors, such as ratio-based indices, is preferred on such substrates [19, 20, 22].

At the interface with biomedical applications, during cell culturing under in vitro conditions, the culture medium is often used as a means to support the growth and development of cell cultures by imitating in vivo conditions. Neurobasal-A-based culture medium (Gibco, Thermo Fisher Scientific, USA) is among the more commonly used culture media for in vitro experiments with neuronal cultures. It contains inorganic salts, mainly NaCl, which crystallise after drying, and leaves visible traces on the surface of the substrate [24]. In general, such evaporation-driven deposition can cause irregular crystal patterns on the surface depending on the droplet volume and surface conditions, and may result in the coffee-ring effect, both of which directly affect the interaction with the 3D microstructures of the surface [25-27]. In the case of MEA substrates with such topography, dried residues represent an artifact of sample preparation, but also a measurable factor that affects the reading of SEM and EDS images. Surface crystals can also affect the quality of the microscopic images of the fixed sample after the electrophysiological part of the experiment.

In this study, SEM/EDS was used to (i) analyse the uniformity of substrate composition within the MEA chip and between multiple chips, and (ii) quantify the effect of dried Neurobasal-A droplets on surface coverage. Using ratio-based indices with factorial statistical comparisons, this study provides a quality control contribution to the optimisation of electrophysiological experiments on 3D microtopographic MEA substrates.

2. Materials and methods

2.1 MEA substrate

In this study, MEA chips, originally presented in a previous study [17], were used as part of an NEI for the extracellular electrophysiology of SGNs. The fabrication procedure was originally described in Huys's doctoral thesis [6]. The chips consist of titanium nitride (TiN)-based electrodes with a diameter of 20 μm, regularly distributed in four zones (zone 1 – zone 4),

with 96 electrodes each arranged in four rows of 24 electrodes spaced 100 µm apart in rows and columns. The surface of each zone is covered with circular micropillars with diameters of 1.0, 1.8, 2.8, and 4.0 µm. The micropillars can be arranged with either 1.2 µm or 2 µm spacing. Each chip is fabricated with only one spacing size. The height of the micropillars and electrodes is 1 µm. The chip scheme is shown in Fig.1.

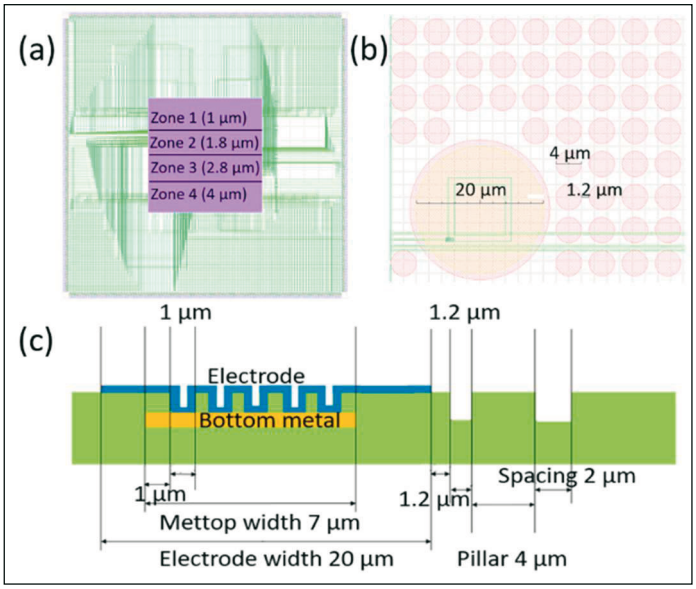

Fig. 1 Schematic view of the chip: (a) zone layout with micropillar dimensions and connections between the electrodes and the pads; (b) enlarged view of a zone 4 segment showing the electrode and surrounding micropillars; (c) cross-sectional schematic of the active chip surface. Reproduced from [17].

Fig. 1 (a) shows a schematic representation of the chip by zone. The active area of the chip is depicted as a 4 mm × 4 mm magenta square, with zones labelled by their micropillar dimensions. The connections between the electrodes and the pads on the edge of the chip, which are located in the area marked in grey, are marked with green lines. The total dimension of the chip is 11 mm × 11 mm.

Fig. 1 (b) shows an enlarged schematic view of the zone 4 segment with the electrode and the micropillars surrounding it. The corresponding dimensions of the diameter of the electrode, pillar, and the distance between the micropillars are indicated.

Fig 1. (c) shows a side cross-section of the active part of the chip. The chip is built on a silicon wafer, with 800 nm high aluminium conductors shown in yellow and represented as green lines in panels (a) and (b). The aluminium conductor is located on a 5 µm high SiO_2 layer marked in green, on which a 50 nm thick layer of SiC is applied, whose role is to form a barrier for the etching process. Using the high-density plasma chemical vapor deposition (HDPCVD) method, an additional layer of SiO_2 3 µm thick, also marked in green, was applied, and the final shaping of the micropillars was performed by the I-line lithography process. The deep-reactive ion etching (DRIE) method was used to create openings in the SiC layer to make contact with the aluminium. The openings are filled with tungsten, and the final formation of the electrode was completed by applying a 100 nm-thick layer of TiN on top of the electrode, marked in blue.

The imaging and measurements were performed on two sets of samples that had previously been sputter coated with a platinum layer of 1 nm for the first set and 2 nm for the second using a Q 150T ES (Quorum Technologies, Lewes, UK) sputter coater to suppress charging and maximise resolution according to the general SEM specimen preparation considerations and conductive coating approaches described in standard protocols [28]. In the

first set of samples (hereinafter referred to as sample set 1), three empty chips (labelled D1-D3) were first imaged using a JSM-7610F SEM system (JEOL, Tokyo, Japan) for visual inspection of the sample to detect impurities or visible mechanical damage. Twelve images were taken on each chip, three in each zone. Each image was framed to contain one electrode surrounded by the corresponding micropillars of the observed zone at a magnification of 1600×, a working distance (WD) of 6.4–6.5 mm, an accelerating voltage of 15 kV, and a 0° tilt, as shown in Fig. 2.

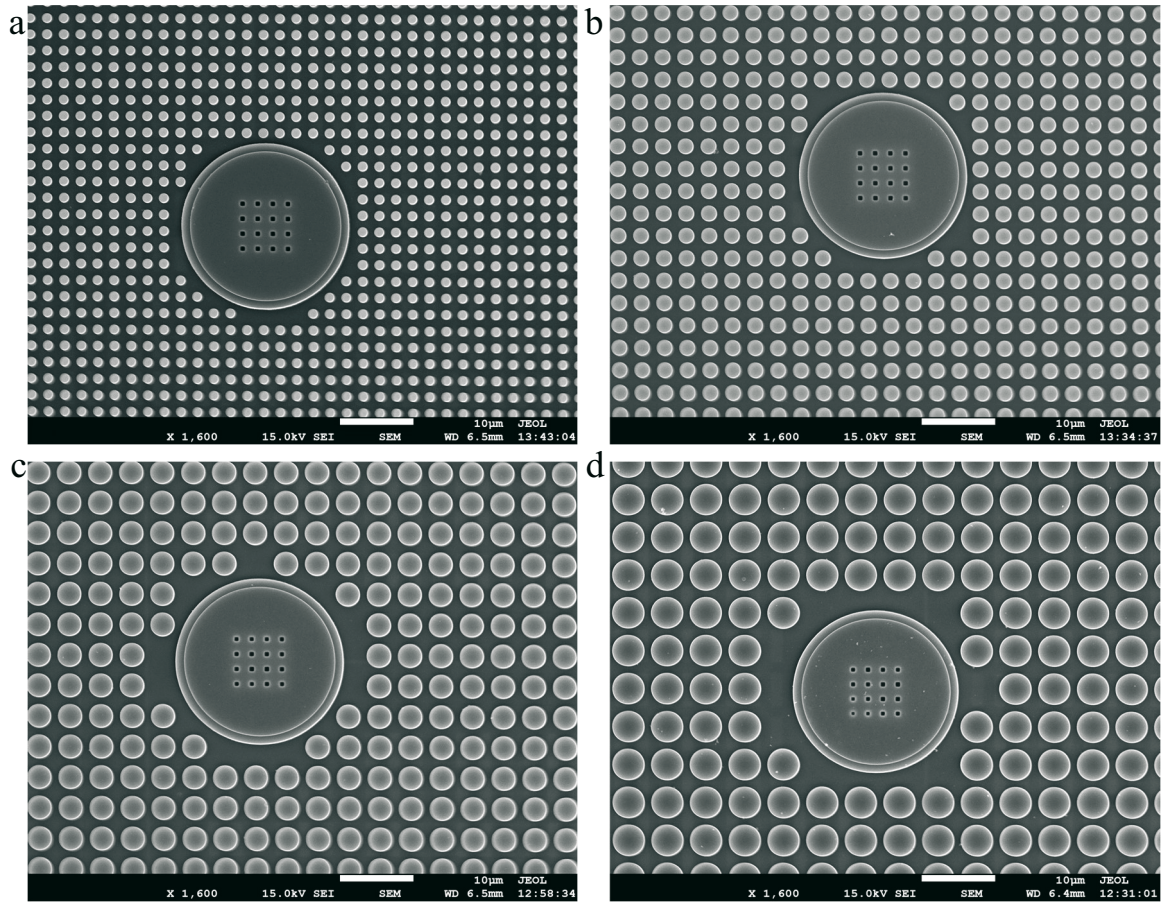

Fig 2 SEM view of micropillar chip zones: (a) zone 1, (b) zone 2, (c) zone 3, (d) zone 4.

2.2 Data acquisition and statistical processing

Quantitative analysis of surface composition on the same set of samples was performed using the Oxford Instruments X-MaxN 80 mm² (Oxford Instruments, Abingdon, UK) operated with Aztec software (version: 5.1; Oxford Instruments, Abingdon, UK) and paired with a SEM device. Three locations (points) were recorded for each zone, which gives 12 spectra per chip, a total of 36, as shown in Table 1. The acquisition settings were chosen with the aim of exciting the lines key to the analysis (O, Al, Si, Ti) with a sufficient energy range and resolution. The EDS spectra were acquired over the selected FOV and reported as intensity (cps/eV) versus X-ray energy. Elemental atomic fractions (at %) were then calculated by the EDS quantification routine from the characteristic peak intensities after background subtraction and standardless matrix correction, yielding the relative elemental composition for the analysed area. The main acquisition parameters (energy range, energy per channel, accelerating voltage, process time, and live time) are listed in Table 2. All settings are the same for all recordings in this section.

Table 1 EDS sampling plan (sample set 1): number of measurement points per zone and total number of spectra per chip.

Chip	Zone				
	Zone 1	Zone 2	Zone 3	Zone 4	Spectra/chip
D1	3	3	3	3	12
D2	3	3	3	3	12
D3	3	3	3	3	12
				Total	36

Table 2 Main SEM/EDS acquisition settings used for sample set 1.

Magnification	1600
Energy range (keV)	20
Energy per channel (eV)	10
Accelerating voltage (kV)	15
Working distance (mm)	6.4
Process time	6
Livetime (s)	30

The following elements were used in the EDS analysis:

- Si: the main building element of the micropillars (SiO_2)
- O: oxide in the substrate (SiO_2)
- Ti: the main building material of the electrodes (TiN).

The elements that were excluded are:

- Al: metal interconnections → geometrically not consistently present in the FOV
- C: present in contaminating particles from the environment
- Pt: sputter coating
- N: low energy line ($K\alpha_N$ = 0.392 keV) → strong absorption → unstable quantification.

The Ti_index was used as the main metric for analysing the chip composition. It represents the relative proportion of titanium atoms in relation to other consistent and dominant elements of the surface matrix (Si and O). The atomic fraction of each element is expressed as *at %*. The Ti_index is defined by equation 1:

$$\text{Ti\_index} = \frac{Ti_{at\,\%}}{Ti_{at\,\%} + Si_{at\,\%} + O_{at\,\%}} \tag{1}$$

Quantification of the composition for sample set 1 was carried out by the EDS module for O, Si and Ti at the chip level between zones and between multiple chips in order to analyse the uniformity of the chip production process. For each chip×zone combination, the Ti_index = Ti / (Ti + Si + O) was calculated as a ratio metric less sensitive to the absolute count-rate and small differences in the WD. The descriptive variables used were the mean (Mean), standard deviation (SD), and coefficient of variation (CoV = SD / Mean) measured at three points on each zone of the chip. Furthermore, ANOVA (Two-Factor with Replication) was conducted with chip and zone as the factors: SS (sum of squares), df (degrees of freedom), MS (SS / df), F (ratio of MSs), P-value, F crit (critical F-value for $\alpha = 0.05$), and η^2 (= SS_effect / SS_total) as the effect size. The table row "Within" refers to the residual variance of the replicates and serves as the denominator for the F-test, and so F- and p-values are not reported. Two-Factor ANOVA with replication was performed on the point-level Ti_index values (3 points per chip×zone cell) in MS Excel, treating points as technical replicates, with the assumptions of independence of observations.

A quantitative analysis of chip surface coverage with the Neurobasal-A-based culture medium (Gibco, Thermo Fisher Scientific, USA) (hereinafter referred to as NB-A) was performed on sample set 2 (four chips: Ch1-Ch4) for two different volumes dropped onto the chip surface: 30 µL and 3 µL, two chips each. The NB-A applied with a micropipette was dried for 24 hours at 24 °C at atmospheric pressure. Each chip was recorded at three points in each zone, and each point was recorded three times, i.e., three spectrum acquisitions were made for each point for greater measurement reliability, as shown in Table 3. Precise shifts along the x and y axes (1 mm) were made because in some cases, due to surface coverage with the NB-A layer, it was difficult to determine the exact recording location and, consequently, the zone, which could have had negative consequences on measurement reliability. The acquisition settings are shown in Table 4.

Table 3 Data acquisition plan for NB-A coverage assessment (sample set 2).

Chip	Volume / µL	Zone (points×repl)				
		Zone 1	Zone 2	Zone 3	Zone 4	Spectra/chip
Ch1	3	3×3 = 9	3×3 = 9	3×3 = 9	3×3 = 9	36
Ch2	3	3×3 = 9	3×3 = 9	3×3 = 9	3×3 = 9	36
Ch3	30	3×3 = 9	3×3 = 9	3×3 = 9	3×3 = 9	36
Ch4	30	3×3 = 9	3×3 = 9	3×3 = 9	3×3 = 9	36
					Total	144

Table 4 EDS acquisition settings for NB-A coverage assessment (sample set 2).

Magnification	700
Energy range (keV)	20
Energy per channel (eV)	10
Accelerating voltage (kV)	15
Process time	6
Livetime (s)	20

The NaCl_index was used as the main metric for analysing the coverage of the chip. This represents the relative proportion of Na and Cl atoms in relation to Si and Al. Due to its presence in both the NB-A and the surface composition, O was excluded from the measurements, and Al was included. Analogously to equation 1, the NaCl_index is defined by equation 2:

$$\text{NaCl\_index} = \frac{Na_{at\,\%} + Cl_{at\,\%}}{Na_{at\,\%} + Cl_{at\,\%} + Si_{at\,\%} + Al_{at\,\%}}. \quad (2)$$

Statistical analysis of the second set, aimed at determining the interaction of the NB-A and chip surface, was carried out according to the same principle as for the first set (Two-Factor ANOVA). The difference in the proportion of observed elements per volume and per zone was analysed in the inferential analysis of sample set 2.

3. Results and discussion

3.1 Chip surface composition

K-lines were observed rather than low-energy L-lines due to less overlap and absorption sensitivity at 15 kV. Fig. 3 provides a demonstrative visual example of EDS measurements for Si, O and Ti (for sample D1, zone 4, point 2) to assess the system's ability to adequately measure the mentioned elements. The resulting visual representation in the form of maps corresponds to the expected distribution of elements over the chip surface.

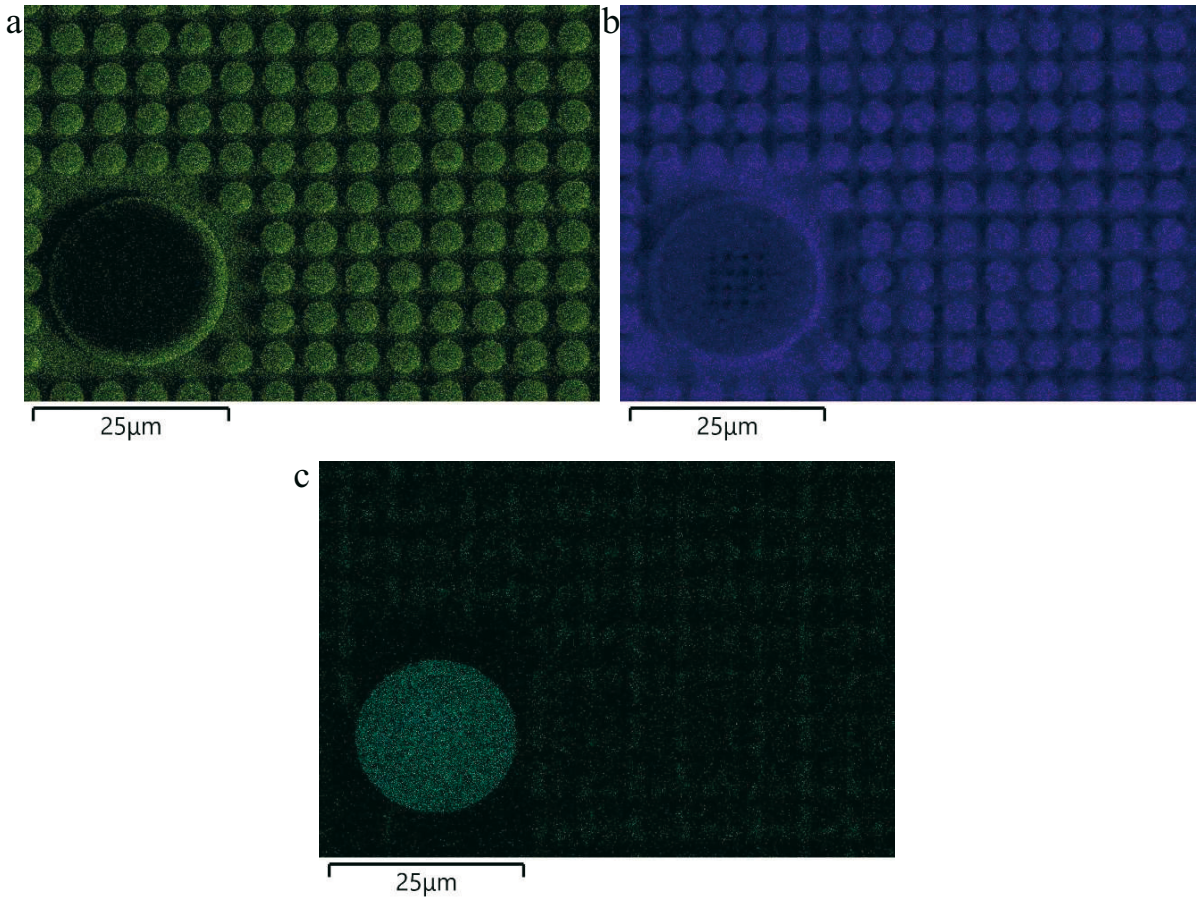

Fig. 3 EDS elemental maps for O (a), Si (b) and Ti (c) for the same FOV. Sample: D1, zone 4, point 2.

The atomic fractions of the elements were measured using EDS for 36 points (one spectrum per point) on sample set 1. An example of such a measurement is given in Table 5. Aluminium was subsequently not included in further statistical processing for the reasons previously stated. The results of the Ti_index measurements for sample set 1 are given descriptively in Table 6, while the results of the ANOVA test are listed in Table 7. For each chip×zone combination, the Ti_index = Ti / (Ti + Si + O) was calculated from three measurements per zone; a higher value indicates the relatively higher contribution of Ti (electrodes) compared to the substrate (SiO_2). The row "Within" represents the variance within the group.

Table 5 Atomic percentage for sample D1–Z4–P2 (the same FOV as in Fig 3).

Spectrum 12 (D1; zone 4; point 2)		
Element	**Line type**	**at %**
O	K series	55.43
Al	K series	9.25
Si	K series	33.41
Ti	K series	1.92
Total		100.00

Table 6 Ti_index per chip and zone (sample set 1).

Chip	Zone	Mean_Ti_idx	SD_Ti_idx	CoV = SD / Mean
D1	Z1	0.0307	0.0030	0.0974
D1	Z2	0.0259	0.0030	0.1168
D1	Z3	0.0234	0.0032	0.1380
D1	Z4	0.0219	0.0024	0.1092
D2	Z1	0.0223	0.0033	0.1461
D2	Z2	0.0238	0.0007	0.0297
D2	Z3	0.0256	0.0009	0.0361
D2	Z4	0.0221	0.0028	0.1281
D3	Z1	0.0255	0.0027	0.1073
D3	Z2	0.0300	0.0022	0.0738
D3	Z3	0.0219	0.0019	0.0880
D3	Z4	0.0189	0.0010	0.0521

Table 7 Two-factor ANOVA with replication for the Ti_index (sample set 1).

Source of variation	SS	df	MS	F	P-value	F crit	η^2
Chip	0.000026	2	0.000013	2.2219	0.1302	3.4028	0.04946
Zone (Z1–Z4)	0.000181	3	0.00006	10.1706	0.0002	3.0088	0.339607
Chip×zone	0.000183	6	0.000031	5.1482	0.0016	2.5082	0.343805
Within	0.000143	24	0.000006				
Total	0.000533						

As shown in Table 6, Ti_index values cover a range of approximately 0.019–0.031 (e.g., D3–Z4 ≈ 0.019; D1–Z1 ≈ 0.031). Within individual chip×zone combinations, the reproducibility is good: the typical CoV is around 3–15 % (e.g., D2–Z2 ≈ 3 %, D2–Z1 ≈ 15 %). Two-factor ANOVA with replication in Table 7 shows that the zone is a significant source of variability ($F = 10.17$; $p = 0.0002$; $\eta^2 = 0.340$), while the main effect of the chip is modest ($F = 2.22$; $p = 0.130$; $\eta^2 = 0.049$). There is also a chip×zone interaction effect ($F = 5.15$; $p = 0.0016$; $\eta^2 = 0.344$), indicating that the zonal profile of the Ti_index differs somewhat between chips. The residual (within-group) variance is small (SS_within = 0.000143; df = 24).

The significant zone effect is consistent with the expected change in the ratio of electrode (Ti) to substrate (SiO_2) in the FOV: zones with a higher proportion of visible substrate give a lower Ti_index, and zones with a higher proportion of electrode give a higher Ti_index. The small main effect of the chip suggests good process uniformity between the chips, while the chip×zone interaction most likely reflects small differences in framing (position relative to the edge of the electrode/pillar) and the microrelief between chips, rather than real compositional changes.

Part of the reason why the Ti_index decreased in zones with larger pillar dimensions can be explained by the metrology of EDS on relief surfaces. As pillars grow, the space between them becomes simpler (shallow, with less sharp transitions), and EDS, due to self-absorption in the "valleys", collects a relatively weaker signal from inter-pillar regions. Although both pillars and "valleys" are made of the same material (Si and O), this topographic bias changes the effective weighting of the substrate contribution versus the flat parts of the frame (e.g., electrode faces/edges), which further lowers the Ti_index in zones with larger pillars. This component does not negatively affect the assessment of process uniformity. All measurements in this section were recorded with the same settings (15 kV, Process time = 6, WD = 6.4–6.5 mm) and a consistent protocol within each zone, so any bias is cancelled out in "chip-within-zone" comparisons. Therefore, it can be concluded that the zone effect is partly caused by the relationship between the surface geometry and metrics, while the chip effect can be considered a reliable indicator of the quality of the manufacturing process.

3.2 Chip surface coverage

In order to avoid mixing the elements of the chip and those that make up the NB-A during the compositional analysis of sample set 2, test recordings and compositional analysis were made on a partially covered segment. For this purpose, EDS maps of the two most abundant elements were recorded: silicon, which makes up the chip, and oxygen, which makes up both the chip and the NB-A that partially covers it, as in Fig. 4. The example of compositional measurement is given in Table 8. The high oxygen content in the composition of the chip surface and NB-A is visible in panel b. In the example from Fig. 4, a magnification of 950× was used for a clearer visual representation, and a test volume of 5 µL of NB-A was applied to the surface. Other parameters used during the acquisition are shown above in Table 4. In addition to oxygen, titanium was also included in the calculation to confirm the ability of the system to observe the electrode in the presence of the NB-A. It was excluded in further measurements because it was impossible to estimate the number of electrodes in the FOV due to the NB-A surface coverage. Unlike in sample set 1, WD was maintained in the range of 6–8 mm throughout all measurements to achieve adequate image focus. Since we use normalised ratios (NaCl / (NaCl + Si + Al)), minimal sensitivity to small changes in WD is expected. A demonstrative SEM image (chip 1, zone 2, point 2, volume 3 µL) is shown in panel c for the same FOV. The map of the spectra confirms the presence of previously defined elements and their suitability for measurements.

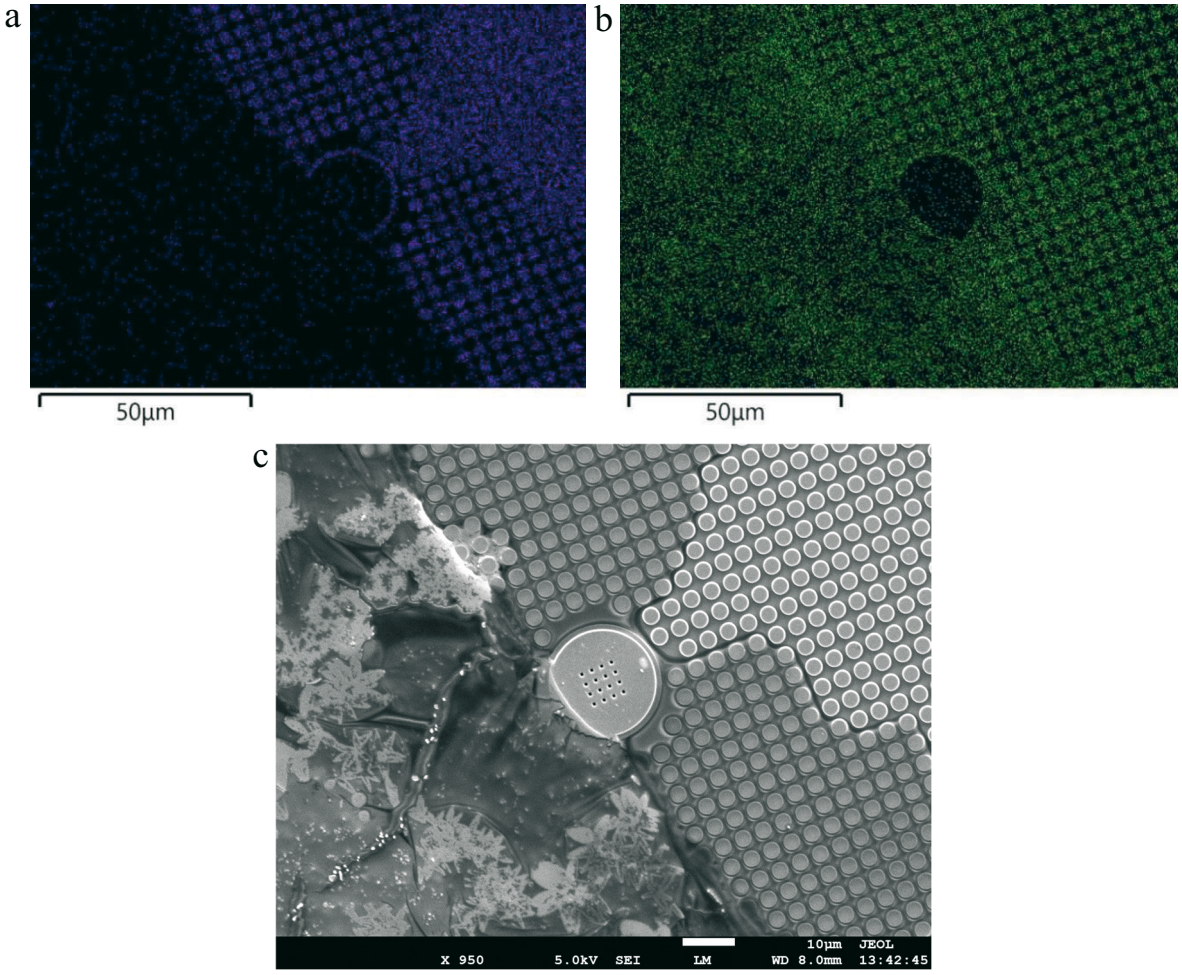

Fig. 4 View of the chip surface (zone 3) partially covered with NB-A: (a) EDS intensity map of Si–Kα; (b) EDS map of O–Kα; (c) SEM image of the same frame.

Table 8 Sample set 2; Test measurement. Na, Al, Si, Cl, Ti and O at % (the same FOV as in Fig. 4).

Test sample (Volume = 5 µL; zone 3)		
Element	**Line type**	**at %**
Na	K series	8.22
Al	K series	0.29
Si	K series	19.80
Cl	K series	3.17
Ti	K series	0.01
O	K series	68.51
Total		100.00

An example of a measured spectrum from sample set 2 without titanium and oxygen is shown in Table 9. As expected, the spectrum of 3 µL of NB-A covering the chip surface is dominated by sodium and chlorine. A spectrum of acquired elements for the same FOV is given in Fig. 5. On the y-axis, the intensity is reported in cps/eV (counts per second per electronvolt), which represents the differential count rate per unit energy. The image confirms the presence of previously defined elements and their suitability for measurements. The EDS module acquisition parameters are given in Table 4.

Table 9 Atomic percentage of Na, Cl, Si and Al (the same FOV as in Fig. 5). Labelled as Spectrum 89.

Spectrum 89 (Ch1; zone 2; point 2)		
Element	**Line type**	**at %**
Na	K series	38.49
Al	K series	3.60
Si	K series	6.85
Cl	K series	51.06
Total		100.00

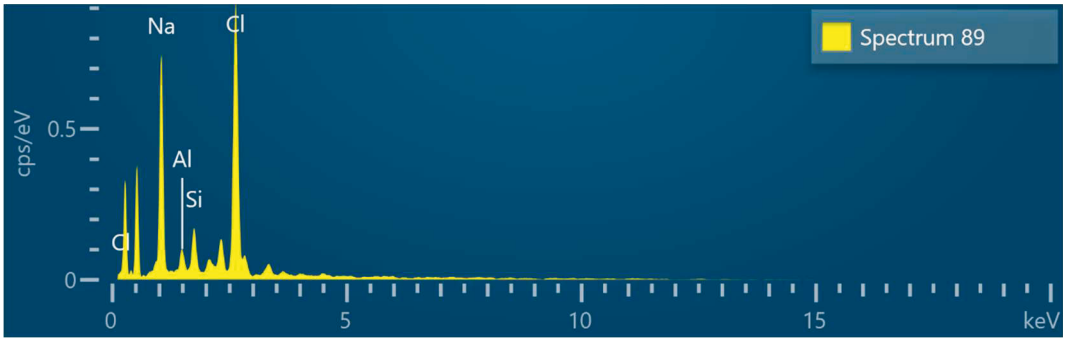

Fig. 5 Spectra of Na, Cl, Si and Al (labelled as Spectrum 89).

A descriptive analysis of the measurement results of the NaCl_index for a total of 144 readings (four chips with 36 measurements each) is listed in Table 10. For each chip×zone combination, the NaCl_index = (Na_at + Cl_at) / (Na_at + Cl_at + Si_at + Al_at), computed from three points per zone (each point aggregated from three spectra). Chips Ch1–Ch2 correspond to 3 µL, and Ch3–Ch4 to 30 µL. The higher NaCl_index indicates greater NB-A residue coverage (lower substrate visibility). Analogous to sample set 1, for each chip-volume-zone combination the mean and standard deviation of the NaCl_index and the coefficient of variation were calculated. Table 11 shows the results of a two-factor ANOVA test with an analysis of the influence of volume (3 µL and 30 µL) and zones (Z1-Z4) on the coverage of the chip surface with NB-A. The reported parameters are SS (sum of squares), df (degrees of freedom), MS (SS / df), F, P-value, F_crit ($\alpha = 0.05$), and η^2 (= SS_effect / SS_total) as effect size.

Table 10 NaCl_index per chip (Ch1–Ch4) and zone (Z1–Z4): mean (Mean), standard deviation (SD); and coefficient of variation (CoV = SD / Mean).

Chip	Volume (µL)	Zone	Mean_NaCl_idx	SD_NaCl_idx	CoV = SD / Mean
Ch1	3	Z1	0.908	0.011	0.0125
Ch1	3	Z2	0.918	0.028	0.0301
Ch1	3	Z3	0.956	0.011	0.0111
Ch1	3	Z4	0.904	0.092	0.1021
Ch2	3	Z1	0.984	0.009	0.0088
Ch2	3	Z2	0.959	0.046	0.0479
Ch2	3	Z3	0.971	0.013	0.0133
Ch2	3	Z4	0.981	0.005	0.0052
Ch3	30	Z1	0.994	0.000	0.0004
Ch3	30	Z2	0.987	0.006	0.0061
Ch3	30	Z3	0.982	0.006	0.0059
Ch3	30	Z4	0.995	0.005	0.0050
Ch4	30	Z1	0.992	0.015	0.0148
Ch4	30	Z2	0.979	0.036	0.0371
Ch4	30	Z3	1.000	0.000	0.0000
Ch4	30	Z4	0.990	0.017	0.0168

Table 11 Two-factor ANOVA with replication for the NaCl_index (factors: volume (3 vs 30 µL); zone 1–zone 4; volume×zone interaction).

Source of Variation	SS	df	MS	F	P-value	F crit	η^2
Volume	0.0072	1	0.0072	8.1948	0.0211	5.3177	0.4773
Zone (Z1–Z4)	0.0006	3	0.0002	0.2088	0.8875	4.0662	0.0365
Volume×zone	0.0003	3	0.0001	0.1162	0.9481	4.0662	0.0203
Within	0.0071	8	0.0009				
Total	0.015133						

As shown in Table 10, the NaCl_index spans roughly 0.904–1.000 (e.g., Ch1–Z4 ≈ 0.904; Ch4–Z3 = 1.000). Reproducibility within chip×zone is good: typical CoV is in the order of 0.5–5% for 30 µL chips (e.g., Ch3–Z2 ≈ 0.006; Ch4–Z1 ≈ 0.015) and ~ 1–10% for 3 µL chips (e.g., Ch2–Z4 ≈ 0.005; Ch1–Z4 ≈ 0.102). Mean values are systematically higher for 30 µL (≈ 0.98–1.00 across zones) than for 3 µL (≈ 0.90–0.98), indicating greater residue coverage after drying at higher initial volume.

The volume main effect is significant ($F = 8.19$, $p = 0.021$, $\eta^2 = 0.477$) whereas the zone showed no systematic effect detected under this design ($F = 0.21$, $p = 0.888$, $\eta^2 = 0.037$), with the same conclusion for the volume×zone ($F = 0.12$, $p = 0.948$, $\eta^2 = 0.020$). The residual variance of SS_within is 0.0071 at df = 8. The results indicate that the NaCl_index increases consistently with the increase in droplet volume from 3 to 30 µL, while the zonal design itself does not systematically change coverage, nor does it modulate the volume effect. Given the sample size of two chips per volume, the zone effects should be interpreted with caution. The main conclusion is that the volume effect is dominant. (Note: Ti is excluded from the NaCl_index denominator to avoid confounding from an unknown electrode fraction in the FOV. The NaCl_index is intended as a practical coverage proxy. When coverage is near-complete, it may saturate.) A graphic representation of the comparison of the NaCl_index for V = 3 µL and V = 30 µL by zones is given in Fig. 6.

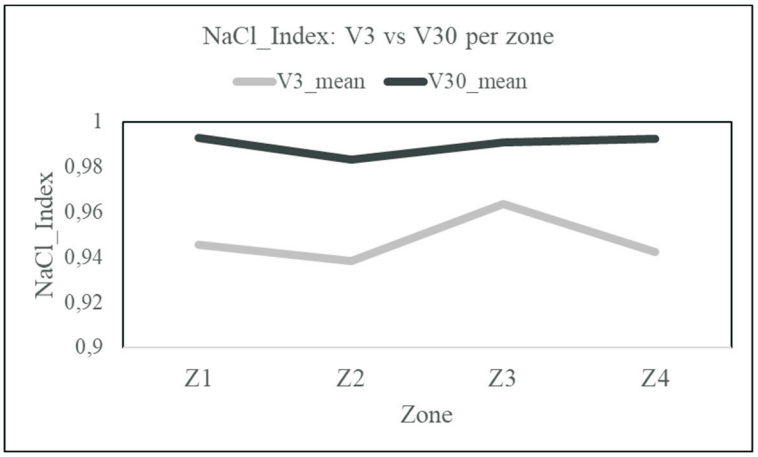

Fig. 6 NaCl_index: V3 vs V30 per zone.

4. Conclusion

In this study, the uniformity of manufactured chips using three-dimensional microtopography of the surface for neuroelectronic applications was examined by analysing their composition using the EDS module and the interaction of the culture medium with the surface of the chip from the aspect of surface coverage.

The analysis performed on sample set 1 (three chips, 36 EDS spectra) showed a high uniformity of composition between different chips (the chip main effect is small $\eta^2 \approx 0.05$), which indicates the good stability of the chip manufacturing process. The differences between the zones are expected due to the influence of the differences in the dimensions of the micropillars, i.e., the three-dimensional structures that define the topography of the surface, on the charging of electrons, which are crucial for the acquisition of data using the EDS technique. Uniformity between chips is a necessary prerequisite for conducting the experiments described in previous related studies [17], ensuring the reliability of measurements and the effect of the chip surface via mechanotaxis on cell cultures in vitro.

The results of testing the interaction of NB-A as a culture medium with the surface of the chip showed a positive relationship between the volume of the medium and the coverage of the surface with the crystalline structures of NaCl that are formed in the drying process. The coverage was shown to be uniform even within different zones of the chip, which is essential to ensure stable in vitro conditions for the growth and development of neuronal cultures during experiments that can last several days or weeks.

Future analyses could aim at determining the critical volume of the culture medium at which there is a difference in coverage between the zones of the chip, since even the smaller volume used in this experiment (3 μL) showed a high level of surface coverage. A critical volume that would result in significant differences between the zones of the chip would imply the existence of the effect of topography defined by the three-dimensional microstructures of the surface, which in this case is overcome by the effect of the volume of the culture medium. Furthermore, in the context of using chips for the purposes described in our previous research [17], it is necessary to examine the minimum volume at which the chip surface is wholly covered, without traces of its surface elements. In addition, to improve the reproducibility and reliability of EDS measurements with a chip covered with culture medium, it is necessary to increase the precision and consistency of FOV targeting. These insights could be useful in respect of achieving uniform conditions for the growth and development of cell cultures, which could lead to optimisation of the experimental protocol and the reliability of experimental results in general.

Acknowledgments

This research was partially supported through the STIM-REI project at the University of Split (UNIST) under Contract Number KK.01.1.1.01.0003, funded by the EU through the European Regional Development Fund (ERDF) – OPKK, and from the "Young Researchers' Career Development Project – Training of Doctoral Students", funded by the Croatian Science Foundation (HRZZ) and the European Social Fund (ESF) of the EU. The authors thank Luka Perković (Faculty of Science, University of Split) for technical assistance and valuable advice when working with SEM/EDS modules.

REFERENCES

[1] Radivojevic, M., Jäckel, D., Altermatt, M., Müller, J., Viswam, V., Hierlemann, A. and Bakkum, D.J., 2016. Electrical identification and selective microstimulation of neuronal compartments based on features of extracellular action potentials. *Scientific reports*, *6*(1), 31332. https://doi.org/10.1038/srep31332

[2] Ronchi, S., Fiscella, M., Marchetti, C., Viswam, V., Müller, J., Frey, U. and Hierlemann, A., 2019. Single-cell electrical stimulation using CMOS-based high-density microelectrode arrays. *Frontiers in neuroscience*, *13*, p.208. https://doi.org/10.3389/fnins.2019.00208

[3] Hahnewald, S., Roccio, M., Tscherter, A., Streit, J., Ambett, R. and Senn, P., 2016. Spiral ganglion neuron explant culture and electrophysiology on multi electrode arrays. Journal of Visualized Experiments: JoVE, (116), p.54538. https://doi.org/10.3791/54538

[4] Senn, P., Roccio, M., Hahnewald, S., Frick, C., Kwiatkowska, M., Ishikawa, M., Bako, P., Li, H., Edin, F., Liu, W. and Rask-Andersen, H., 2017. NANOCI—nanotechnology based cochlear implant with gapless interface to auditory neurons. Otology & Neurotology, 38(8), pp. e224-e231. https://doi.org/10.1097/MAO.0000000000001439

[5] Obien, M.E.J., Deligkaris, K., Bullmann, T., Bakkum, D.J. and Frey, U., 2015. Revealing neuronal function through microelectrode array recordings. *Frontiers in neuroscience*, *8*, p.423. https://doi.org/10.3389/fnins.2014.00423

[6] Huys, R., 2011. CMOS Microelectrode Arrays for Neurophysiological Applications (CMOS micro-electrode arrays voor neurofysiologische toepassingen).

[7] Huys, R., Braeken, D., Jans, D., Stassen, A., Collaert, N., Wouters, J., Loo, J., Severi, S., Vleugels, F., Callewaert, G. and Verstreken, K., 2012. Single-cell recording and stimulation with a 16k micro-nail electrode array integrated on a 0.18 μm CMOS chip. *Lab on a Chip*, *12*(7), pp.1274-1280. https://doi.org/10.1039/c2lc21037a

[8] Braeken, D., Jans, D., Huys, R., Stassen, A., Collaert, N., Hoffman, L., Eberle, W., Peumans, P. and Callewaert, G., 2012. Open-cell recording of action potentials using active electrode arrays. *Lab on a Chip*, *12*(21), pp.4397-4402. https://doi.org/10.1039/c2lc40656j

[9] Braeken, D., Huys, R., Loo, J., Bartic, C., Borghs, G., Callewaert, G. and Eberle, W., 2010. Localized electrical stimulation of in vitro neurons using an array of sub-cellular sized electrodes. *Biosensors and Bioelectronics*, *26*(4), pp.1474-1477. https://doi.org/10.1016/j.bios.2010.07.086

[10] Lutolf, M.P. and Hubbell, J.A., 2005. Synthetic biomaterials as instructive extracellular microenvironments for morphogenesis in tissue engineering. Nature biotechnology, 23(1), pp.47-55. https://doi.org/10.1038/nbt1055

[11] Bettinger, C.J., Langer, R. and Borenstein, J.T., 2009. Engineering substrate topography at the micro-and nanoscale to control cell function. Angewandte Chemie International Edition, 48(30), pp.5406-5415. https://doi.org/10.1002/anie.200805179

[12] Hoffman-Kim, D., Mitchel, J.A. and Bellamkonda, R.V., 2010. Topography, cell response, and nerve regeneration. Annual review of biomedical engineering, 12(1), pp.203-231. https://doi.org/10.1146/annurev-bioeng-070909-105351

[13] Nguyen, A.T., Sathe, S.R. and Yim, E.K., 2016. From nano to micro: topographical scale and its impact on cell adhesion, morphology and contact guidance. Journal of Physics: Condensed Matter, 28(18), 183001. https://doi.org/10.1088/0953-8984/28/18/183001

[14] Mattotti, M., Micholt, L., Braeken, D. and Kovačić, D., 2015. Characterization of spiral ganglion neurons cultured on silicon micro-pillar substrates for new auditory neuro-electronic interfaces. *Journal of neural engineering*, *12*(2), p.026001. https://doi.org/10.1088/1741-2560/12/2/026001

[15] Radotić, V., Braeken, D., Drviš, P., Mattotti, M. and Kovačić, D., 2018. Advantageous environment of micro-patterned, high-density complementary metal–oxide–semiconductor electrode array for spiral ganglion neurons cultured in vitro. *Scientific reports*, *8*(1), p.7446. https://doi.org/10.1038/s41598-018-25814-w

[16] Radotić, V., Bedalov, A., Drviš, P., Braeken, D. and Kovačić, D., 2019. Guided growth with aligned neurites in adult spiral ganglion neurons cultured in vitro on silicon micro-pillar substrates. *Journal of neural engineering*, *16*(6), p.066037. https://doi.org/10.1088/1741-2552/ab2968

[17] Delipetar, B., Žarković Krolo, J., Bedalov, A. and Kovačić, D., 2025. A Neuroelectronic Interface with Microstructured Substrates for Spiral Ganglion Neurons Cultured In Vitro: Proof of Concept. *Biosensors*, *15*(4), p.224. https://doi.org/10.3390/bios15040224

[18] Walther, T., 2024. Recent improvements in quantification of energy-dispersive X-ray spectra and maps in electron microscopy of semiconductors. *Applied Research*, *3*(6), p.e202300128. https://doi.org/10.1002/appl.202300128

[19] Newbury, D. and Ritchie, N., 2011. Is SEM/EDS Quantitative?. *Microscopy and Microanalysis*, *17*(S2), pp.558-559. https://doi.org/10.1017/S1431927611003667

[20] Newbury, D.E. and Ritchie, N.W., 2019. Electron-excited X-ray microanalysis by energy dispersive spectrometry at 50: Analytical accuracy, precision, trace sensitivity, and quantitative compositional mapping. *Microscopy and Microanalysis*, *25*(5), pp.1075-1105. https://doi.org/10.1017/S143192761901482X

[21] Rönnhult, T., Brox, B. and Fritze, G., 1987. The influence of surface topography on the x-ray intensity in electron microprobe analysis (EDS/WDS). *Scanning*, *9*(2), pp.81-87. https://doi.org/10.1002/sca.4950090205

[22] Shirley, B. and Jarochowska, E., 2022. Chemical characterisation is rough: the impact of topography and measurement parameters on energy-dispersive X-ray spectroscopy in biominerals. *Facies*, *68*(2), p.7. https://doi.org/10.1007/s10347-022-00645-4

[23] EDAX. EDS/WDS Geometry and the Famous Take-off Angle [Technical note on the Internet]. [cited 2026 Jan 18]. Available at: https://www.edax.com/-/media/ametekedax/files/integrated_technologies/technical_notes/edswds-geometry-and-the-famous-take-off-angle-technical-note.pdf

[24] Thermo Fisher Scientific (Gibco). Neurobasal™-A Medium (1X) liquid—Media formulation [Internet]. Waltham (MA): Thermo Fisher Scientific; [cited 2026 Jan 18]. Available from: https://www.thermofisher.com/us/en/home/technical-resources/media-formulation.256.html

[25] Deegan, R.D., Bakajin, O., Dupont, T.F., Huber, G., Nagel, S.R. and Witten, T.A., 1997. Capillary flow as the cause of ring stains from dried liquid drops. Nature, 389(6653), pp.827-829. https://doi.org/10.1038/39827

[26] Hu, H. and Larson, R.G., 2006. Marangoni effect reverses coffee-ring depositions. *The Journal of Physical Chemistry B*, *110*(14), pp.7090-7094. https://doi.org/10.1021/jp0609232

[27] Mampallil D, Eral HB. A review on suppression and utilization of the coffee-ring effect. Advances in colloid and interface science. 2018 Feb 1; 252:38-54. https://doi.org/10.1016/j.cis.2017.12.008

[28] Fischer, E.R., Hansen, B.T., Nair, V., Hoyt, F.H., Schwartz, C.L. and Dorward, D.W., 2024. Scanning Electron Microscopy. *Current Protocols*, 4(5), p.e1034. https://doi.org/10.1002/cpz1.1034

Submitted: 30.01.2026

Accepted: 06.02.2026

Boris Delipetar*
Faculty of Electrical Engineering, Mechanical Engineering and Naval Architecture, University of Split, Ruđera Boškovića 32, 21000 Split, Croatia

Ivana Weber
Damir Kovačić
Faculty of Science, University of Split, Ruđera Boškovića 33, 21000 Split, Croatia

*Corresponding author:
Boris.Delipetar.00@fesb.hr